Supplementary Information

Enhanced H_2S Gas Detection Using Low-Cost Carbon Loaded $CuCrO_2$-CuO Nanomaterials

Shaik Ruksana[a], Seetha Lakshmy[a], Amit Kumar[b], Chandra Shekhar Sharma[a,*], Mahesh Kumar[b,*]

[a]*Department of Chemical Engineering, Indian Institute of Technology Hyderabad, Hyderabad, Telangana, 502285, India*

[b]*Department of Electrical Engineering, Indian Institute of Technology Jodhpur, Jodhpur, Rajasthan, 342037, India*

Corresponding author E-mail: cssharma@che.iith.ac.in (C. S. Sharma), mkumar@iitj.ac.in (M. Kumar)

Experimental method

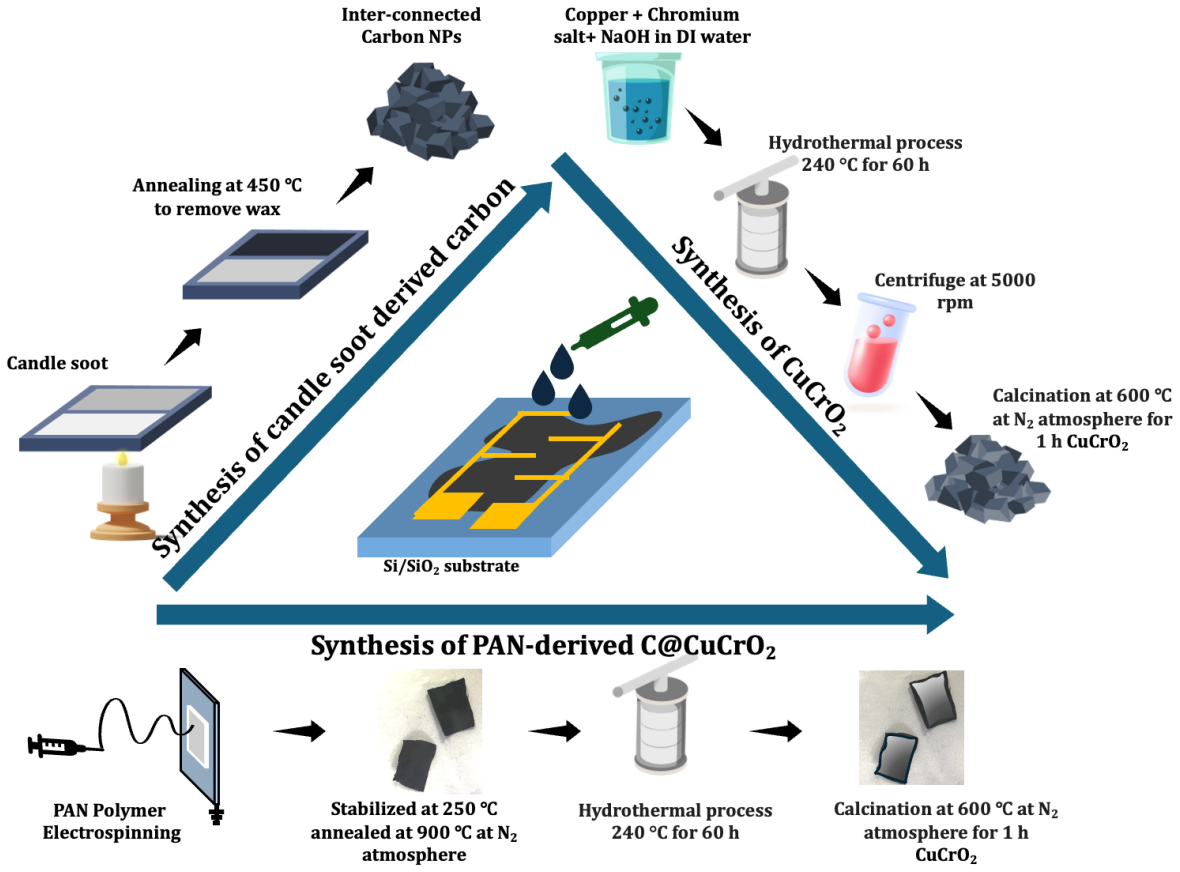

Fig. S1 Synthesis process of C-loaded $CuCrO_2$ and sensor fabrication.

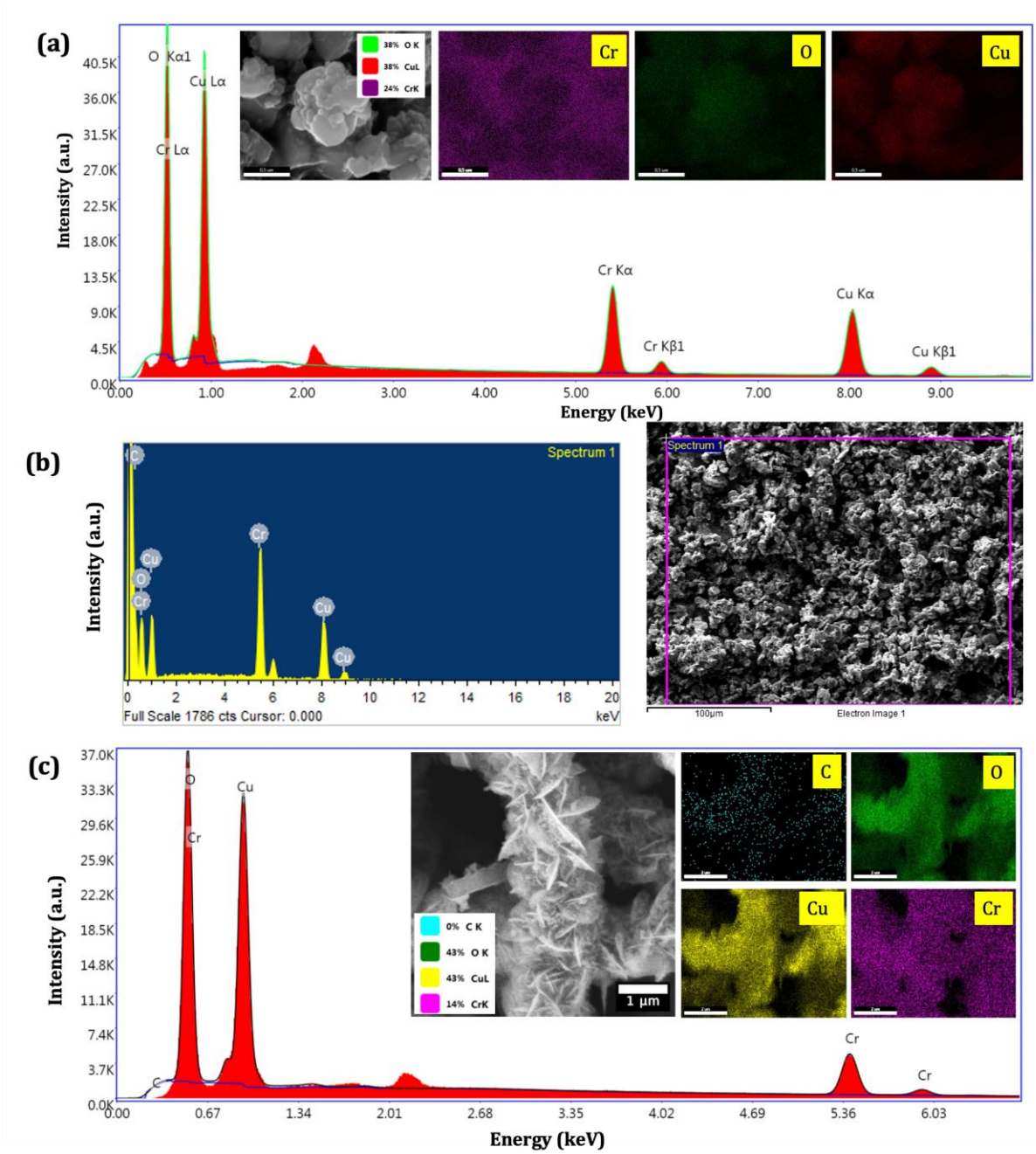

Fig. S2 EDS analysis of (a) $CuCrO_2$, CS@$CuCrO_2$ and (c) PAN-derived CNF@$CuCrO_2$.

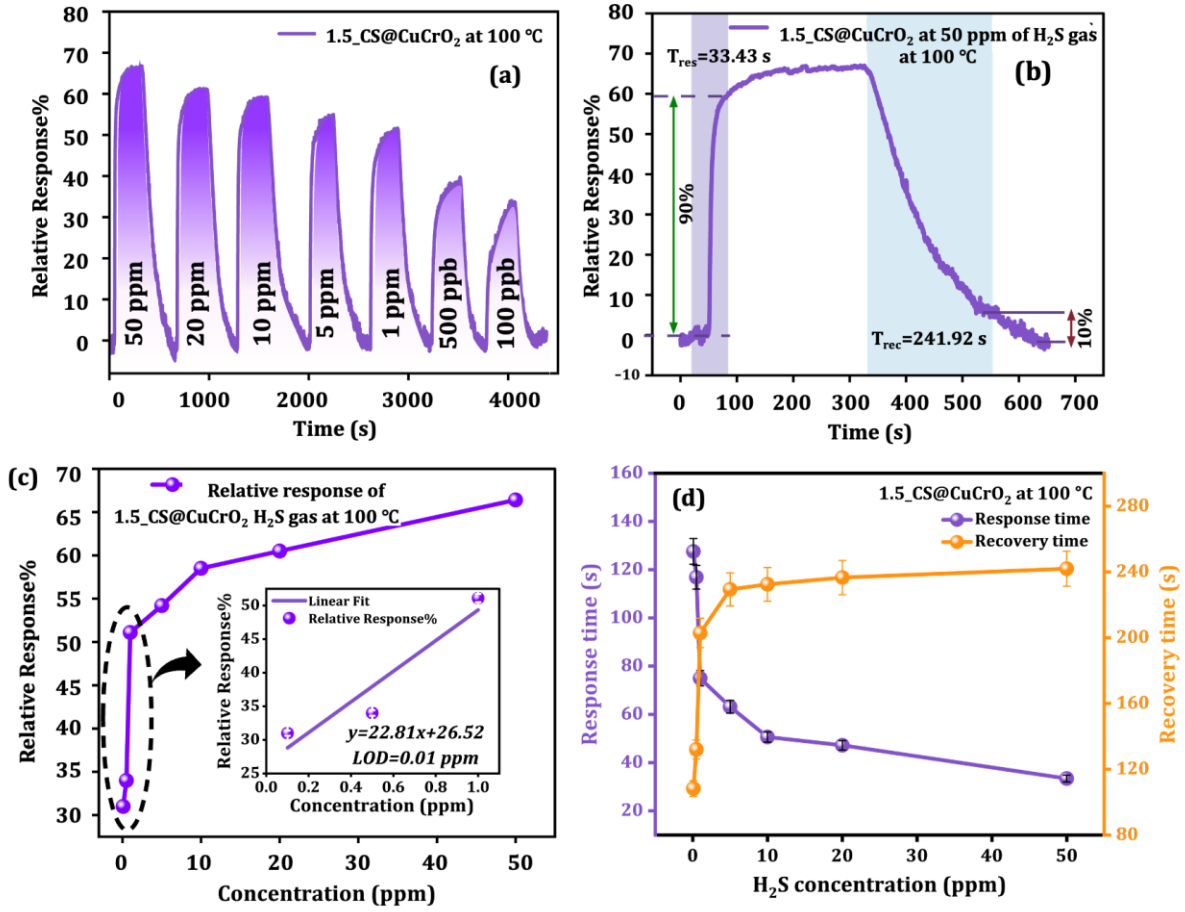

Fig. S3 (a) Response plot of 1.5_CS@$CuCrO_2$ at various concentration of H_2S gas. (b) Response and recovery time of 1.5_CS@$CuCrO_2$ at 50 ppm for H_2S gas at 100 °C. (c) Calculated LOD for 1.5_CS@$CuCrO_2$ for H_2S gas at 100 °C. (d) Response and recovery time of 1.5_CS@$CuCrO_2$ for difference concentration of H_2S gas at 100 °C.

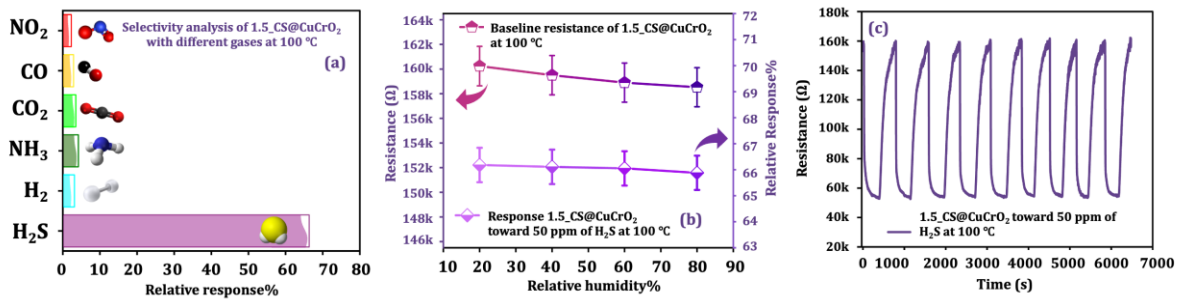

Fig. S4 (a) Selectivity analysis with other gases for CS@$CuCrO_2$ at 100 °C. (b) Effect of relative humidity (±3.5% RH at 30°C ± 4°C) on the baseline resistance and response of

CS@$CuCrO_2$ 50 ppm of H_2S gas at 100 °C. (c) Repeatability for CS@$CuCrO_2$ for 9 cycles for 50 ppm of H_2S gas at 100 °C.

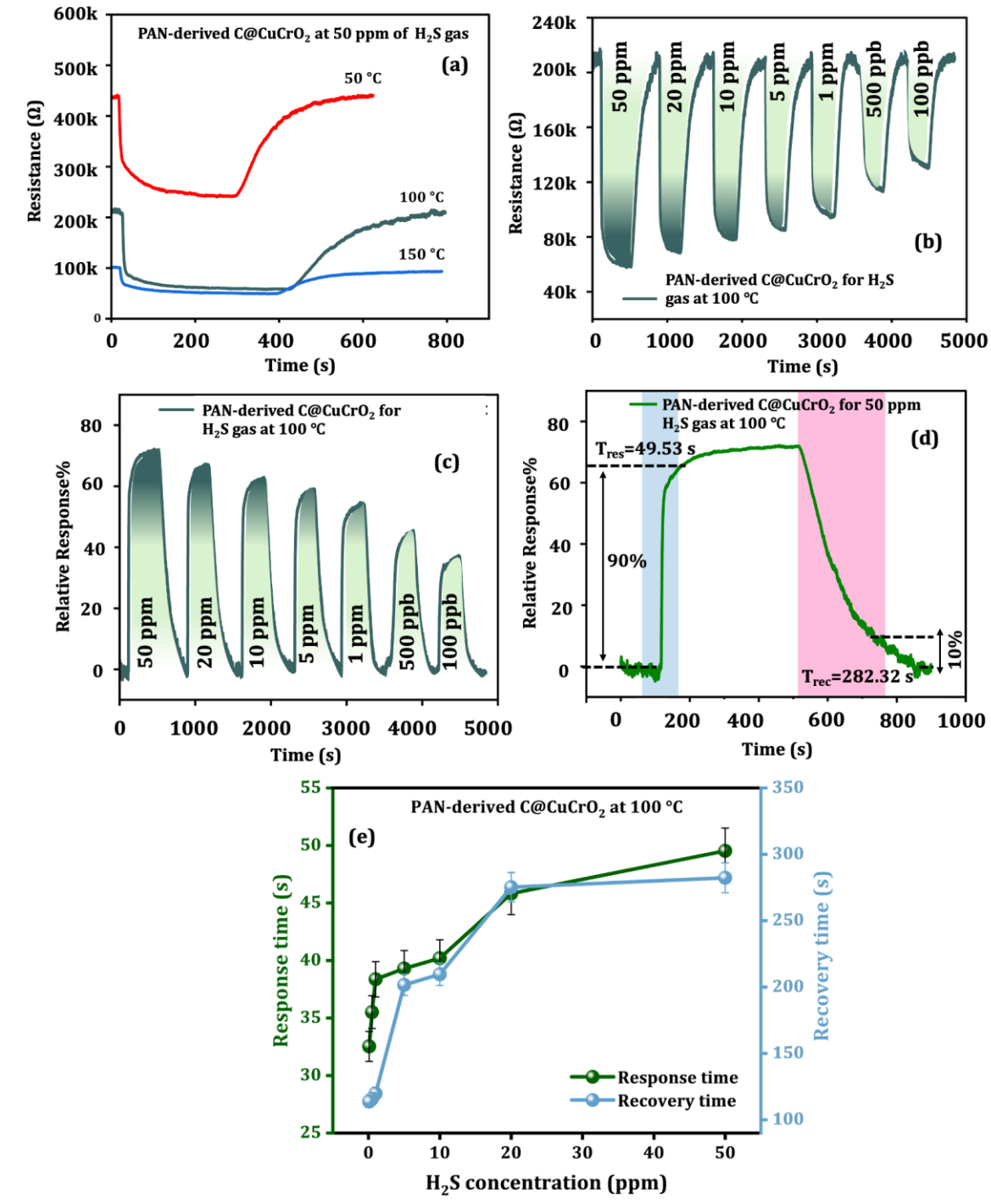

Fig. S5 (a) Resistance changes for 50 ppm of H_2S gas for PAN-derived C@$CuCrO_2$ exposed various temperatures. (b) Resistance and gas sensing response plot of PAN-derived C@$CuCrO_2$ at different concentrations of H_2S gas at 100 °C. (c) Calculated response for PAN-derived

C@$CuCrO_2$ to varying concentrations of H_2S gas at 100 °C. (d) Response and recovery time of PAN-derived C@$CuCrO_2$ at 50 ppm for H_2S gas at 100 °C. (e) Response and recovery time of PAN-derived C@$CuCrO_2$ for various concentration of H_2S gas at 100 °C.

To know the optimum temperature, PAN-derived C@$CuCrO_2$ was exposed to 50 ppm of H_2S gas at different temperatures. Fig. S5a indicates the sensor's performance was adequate at 100 °C for 50 ppm of H_2S gas, following all the studies at 100 °C. Fig. S5b represents the behavior of the PAN-derived C@$CuCrO_2$, which was tested against H_2S gas varying the concentration from 50 ppm to 100 ppb. The calculated response based on resistance change indicates a 70.98% response for 50 ppm of H_2S gas, comparatively higher than the CS@$CuCrO_2$ (Fig. S5c). At 500 and 100 ppb of H_2S gas, the sensor responded effectively with 49% and 40%, respectively. The consistency at lower concentrations confirms the sensitivity to H_2S gas. The enhanced performance is attributed to the modified surface area and uniform growth of $CuCrO_2$ petals on PAN-derived carbon nanofibers, which offers a more active site for the adsorption of H_2S gas [1–3]. To analyze the response time and recovery time, 50 ppm of H_2S gas was evaluated further to attain 49 s and 282.2 s of response and recovery time, respectively (Fig. S5d). The response and recovery time for various concentration of H_2S is calculated (Fig. S5e),
the data interprets as the concentration of H_2S is increased, the sensor is taking more time to sense the gas. The prolonged response and recovery times for PAN-derived C@$CuCrO_2$ can be attributed to the modified structure of the C@$CuCrO_2$, as represented in the FESEM analysis, the uniform growth of the $CuCrO_2$ on the PAN-derived CNF.

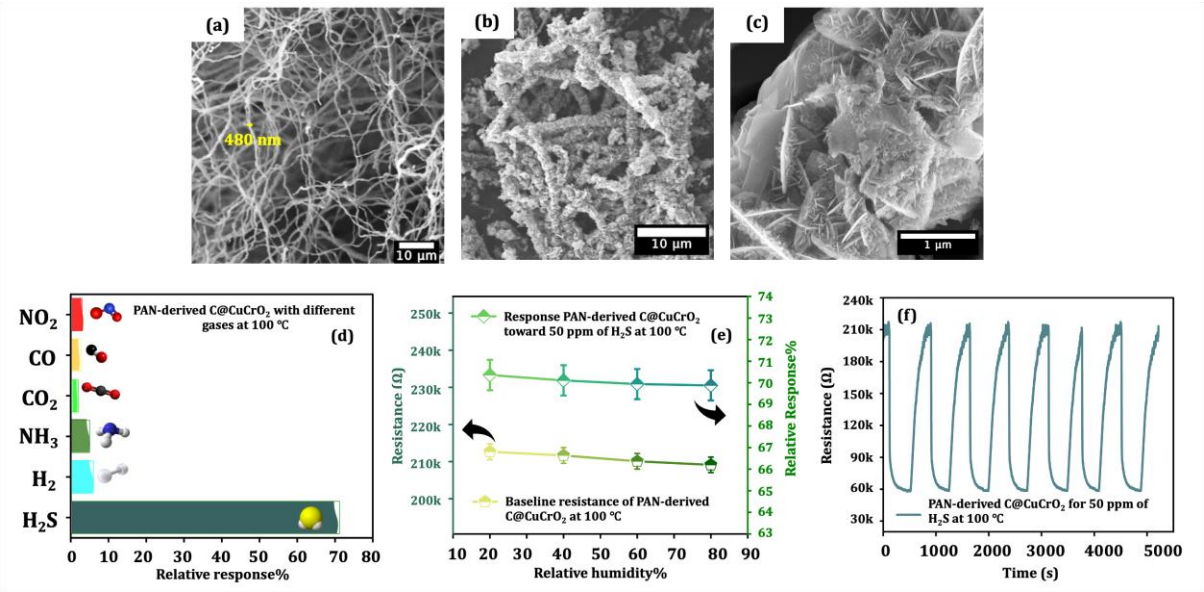

Fig. S6 FESEM micrographs of (a) PAN-derived CNF and (b & c) $CuCrO_2$ grown on PAN-derived CNF. (d) Selectivity analysis with other gases for PAN-derived C@$CuCrO_2$ at 100 °C. (e) Effect of relative humidity (±3.5% RH at 30°C ± 4°C) on the baseline resistance and response of PAN-derived C@$CuCrO_2$ for 50 ppm of H_2S gas at 100 °C. (f) Repeatability for PAN-derived C@$CuCrO_2$ for 7 cycles for 50 ppm of H_2S gas at 100 °C.

Fig. S6a shrinkage in the CNF nanofiber is due to the exposure to elevated temperature and conversion of polymer to carbon at 900 °C in the N_2 atmosphere. The average diameter of PAN-derived CNF was reported as ~480 nm. The *in-situ* growth of $CuCrO_2$ on CNF can be seen in Fig. S6b and S6c. These $CuCrO_2$ grown petals on PAN-derived CNF result in surface roughness, enhancing the active gas adsorption sites.

Table 1. Comparison of carbon based $CuCrO_2$ gas sensor with literature.

S. No.	Material utilized	Gas	Operating Temp. °C	Response %	Response time (s)	Recovery time (s)	Ref.
1	$CuCrO_2$ nanoparticles	H_2S	100 °C	~40% (50 ppm)	30	60	[4]
2	$CuGaO_2$ thin film	H_2S	100 °C	~25% (50 ppm)	66	258	[5]
3	PAN/Nickel Nanofiber on QCM	Methanol	RT	389+3.8 Hz/SCCM	288	251	[6]
4	PANI/N-GQD/Hollow In_2O_3 nanofiber	NH_3	RT	15.2% (1 ppm)	-	-	[7]
5	1.5_CS@$CuCrO_2$	H_2S	100 °C	66.4% (50 ppm)	82.78	221.79	Present work
6	PAN-derived C@$CuCrO_2$	H_2S	100 °C	70.49% (50 ppm)	97.81	949.2	Present work

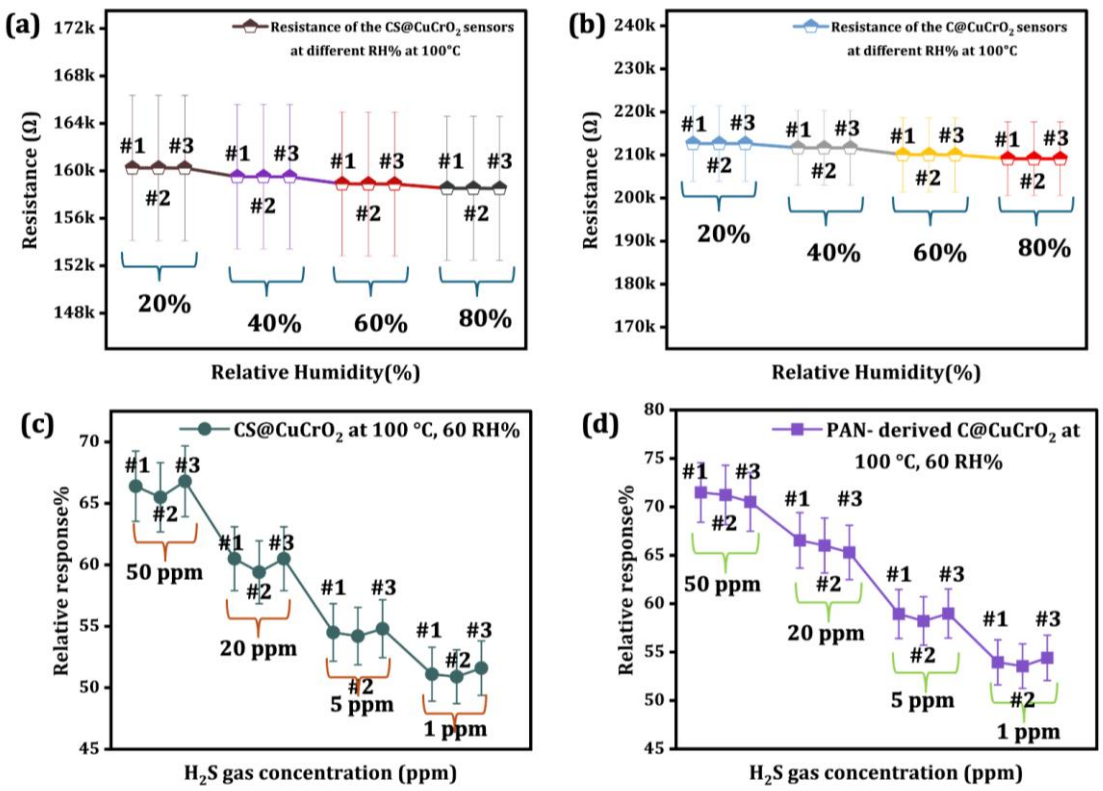

Fig. S7 Monitoring baseline resistance for various samples of (a) CS@$CuCrO_2$ and (b) PAN-derived C@$CuCrO_2$ operated at various humid conditions at 100 °C. Relative response of 3 samples of (c) CS@$CuCrO_2$ and (d) PAN-derived C@$CuCrO_2$ kept at 60% RH for different concentration of H_2S gas.

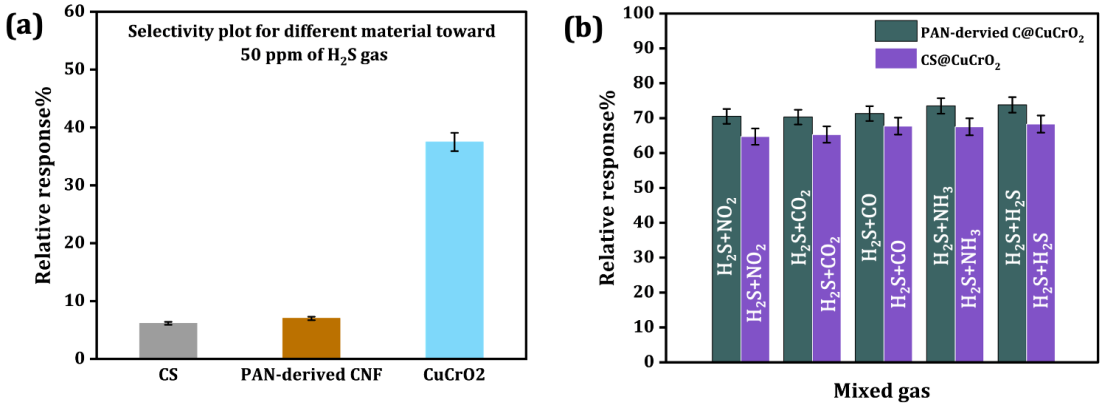

Fig. S8 Selectivity plot for (a) different materials toward 50 ppm of H_2S gas. (b) Selectivity plot both sensors CS@$CuCrO_2$ and PAN-derived C@$CuCrO_2$ with mixed gases.

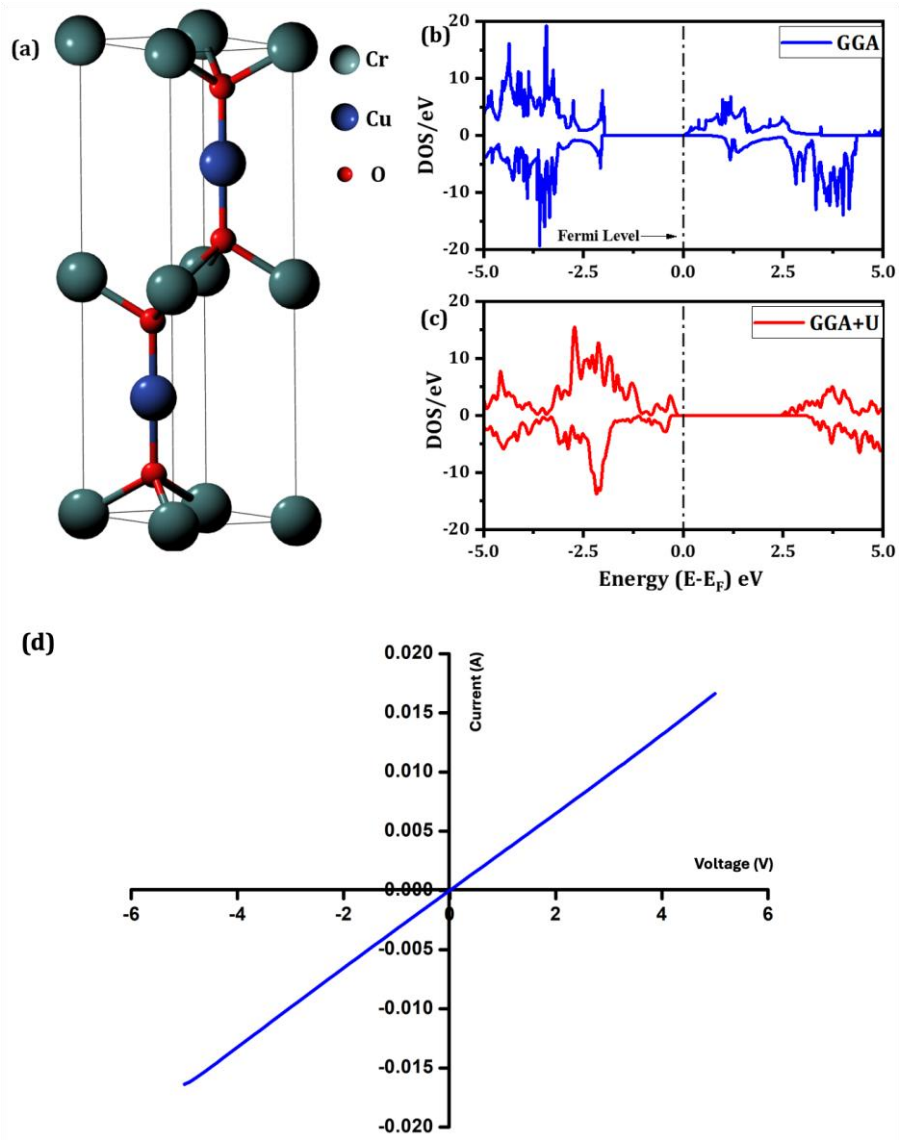

Fig. S9 (a) DFT-optimized unit cell of bulk $CuCrO_2$ and DOS plots of bulk $CuCrO_2$ calculated using (b) GGA and (c) GGA+U hybrid functional. (d) IV characteristics of candle soot.

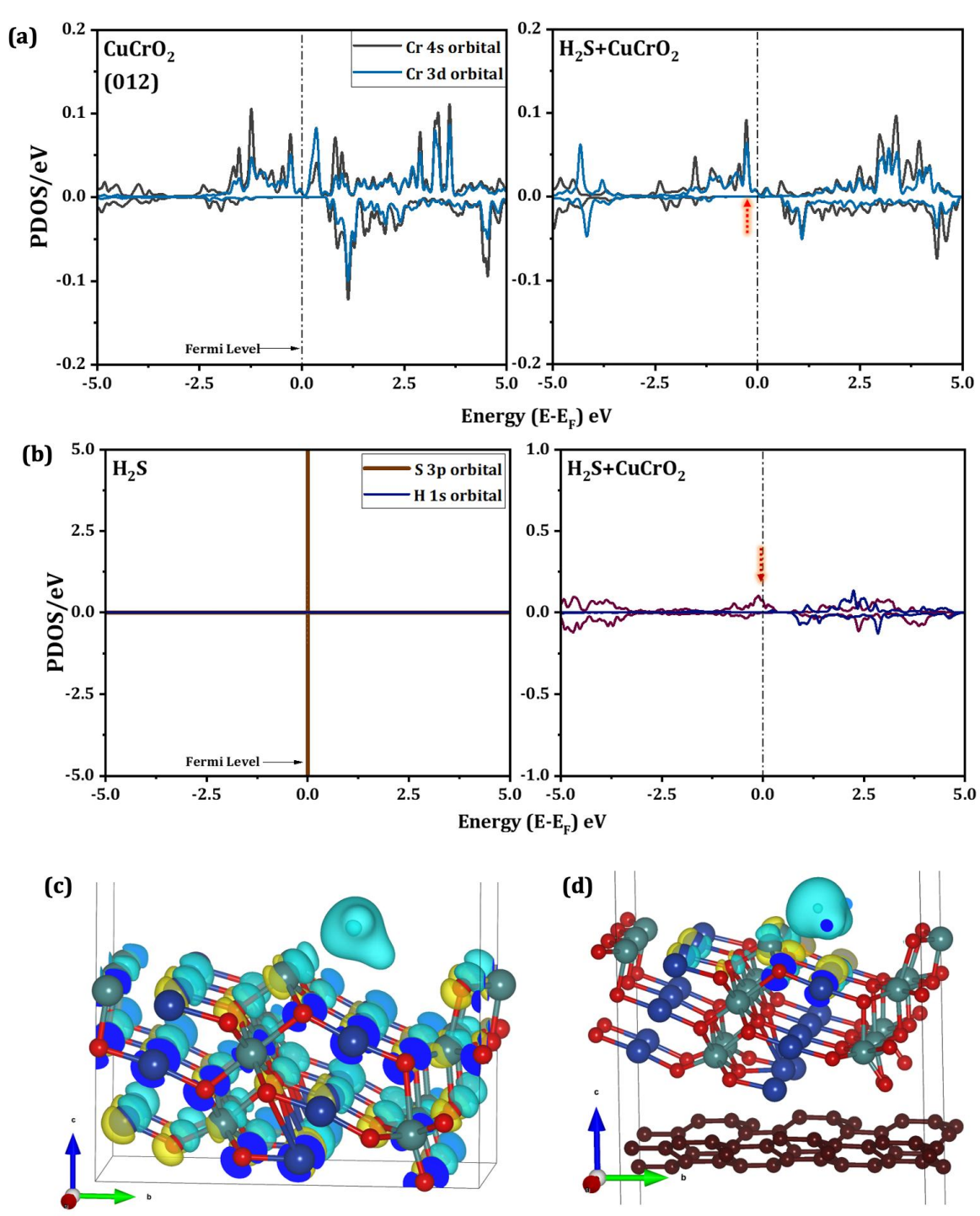

Fig. S10 PDOS plots comparing the valence orbitals of (a) Cu and Cr of $CuCrO_2$ before (left panel) and after (right panel) H_2S interaction (b) H atom of H_2S in the isolated state (left) and after interaction (right) with the $CuCrO_2$. Charge density difference iso-surface plot of H_2S adsorbed (c) $CuCrO_2$ and (d) $CuCrO_2$@C with the iso-surface value of 0.06 and 0.03 e $Å^{-3}$,

respectively. The cyan color around the H_2S indicates the charge loss while the yellow color around the Cr atom indicates charge gain.

References:

(1) S. Hou, R. Pang, S. Chang, L. Ye, J. Xu, X. Wang, Y. Zhang, Y. Shang, A. Cao, Synergistic CNFs/CoS_2/MoS_2 Flexible Films with Unprecedented Selectivity for NO Gas at Room Temperature, *ACS Appl Mater Interfaces* 12 (2020) 29778–29786. https://doi.org/10.1021/acsami.0c05953

(2) Q. Duan, W. Zhang, L. Li, B. Ying, T. Li, B. Chen, H.Y. Li, H. Liu, W-CeO2 nanospheres gas sensor array for accurate and selective H_2S detection in exhaled breath, *Chem Eng J* 479 (2024) 147748. https://doi.org/10.1016/j.cej.2023.147748

(3) A.N. Begi, S. Hussain, J.N.O. Amu-Darko, S. Shah, W. Junhao, X. Zhang, K. Yusuf, R.K. Manavalan, G. Qiao, G. Liu, Low-concentration H_2S gas sensors based on MOF-derived Co_3O_4 nanomaterials, *Sens Actuators A Phys* 378 (2024) 115776. https://doi.org/10.1016/j.sna.2024.115776

(4) R. Zhang, Z. Deng, L. Shi, M. Kumar, J. Chang, S. Wang, X. Fang, W. Tong, G. Meng, Pt-Anchored $CuCrO_2$ for Low-Temperature-Operating High-Performance H_2S Chemiresistors, *ACS Appl Mater Interfaces* 14 (2022) 24536–24545. https://doi.org/10.1021/acsami.2c00619

(5) A. Kumar, S. Barala, M.M. Ganaie, M. Kumar, Delafossite $CuGaO_2$ nanomaterial-based room temperature H_2S selective gas sensor, *J Mater Chem C Mater* 12 (2024) 16854–16863. https://doi.org/10.1039/d4tc02872d

(6) Y.M. Rohman, R. Sukowati, A. Priyanto, D.A. Hapidin, D. Edikresnha, K. Khairurrijal, Quartz Crystal Microbalance Coated with Polyacrylonitrile/Nickel Nanofibers for High-Performance Methanol Gas Detection, *ACS Omega* 8 (2023) 13342–13351. https://doi.org/10.1021/acsomega.3c00760

(7) N. Indarit, Y.H. Kim, N. Petchsang, R. Jaisutti, Highly sensitive polyaniline-coated fiber gas sensors for real-time monitoring of ammonia gas, *RSC Adv* 9 (2019) 26773–26779. https://doi.org/10.1039/c9ra04005f